Structure *15*

Supplemental Data

Structural and Thermodynamic Basis for Enhanced DNA Binding by a Promiscuous Mutant EcoRI Endonuclease

Paul J. Sapienza, John M. Rosenberg, and Linda Jen-Jacobson

Table S1. Torsion and Phase Angles[a] Associated with the DNA Backbone of Nucleic Acids in Wild-Type (Black) and A138T (Red) EcoRI Specific Complexes

Torsions (°)	χ C1'-N	γ C5'-C4'	δ C4'-C3'	ε C3'-O3'	ζ O3'-P	α P-O5'	β O5'-C5'	Phase	Pucker
C	-105.7	51.7	139.3	-162.8	-102.6	-	-178.4	163.4	C2'-endo
	-106.3	57.2	141.9	-160.4	-96.8	-	177.6	168.4	C2'-endo
G	-112.4	53.3	119.0	168.1	-112.4	-66.8	165.8	132.4	C1'-exo
	-99.4	49.5	119.3	171.2	-121.3	-64.5	164.8	133.2	C1'-exo
C	-111.8	51.7	138.4	175.3	-96.2	-56.7	-171.2	161.2	C2'-endo
	-110.8	49.7	139.9	174.0	-92.7	-59.3	-171.5	167.3	C2'-endo
G	-122.1	50.6	132.1	-174.6	-113.3	-59.3	-177.1	150.4	C2'-endo
	-128.9	51.2	130.9	-169.3	-115.6	-58.1	176.2	142.5	C1'-exo
A	-107.6	45.4	140.8	-150.1	-74.2	-55.0	-175.8	164.6	C2'-endo
	-102.9	44.7	144.7	-153.9	-77.2	-58.2	-170.1	172.0	C2'-endo
A	-91.9	56.8	130.4	-79.0	128.2	-90.5	171.4	140.0	C1'-exo
	-90.4	44.9	131.8	-80.3	124.7	-79.8	170.7	139.8	C1-exo
T	-131.4	33.3	103.3	-155.0	-100.9	-73.4	145.3	78.2	O4'-exo
	-133.4	31.1	102.9	-155.8	-103.5	-72.4	143.0	74.4	O4'-endo
T	-105.4	51.5	139.6	-173.5	-95.6	-52.8	179.8	165.5	C2'-endo
	-101.8	48.2	140.9	-175.1	-93.8	-47.5	178.2	172.6	C2'-endo
C	-106.7	49.1	127.2	-157.3	-142.9	-49.1	168.4	144.0	C2'-endo
	-100.2	50.2	144.7	-125.1	178.2	-56.5	165.2	151.8	C2'-endo
G	-115.7	43.8	142.0	-172.9	-97.3	-50.9	168.2	170.9	C2'-endo
	-120.5	36.1	140.1	-172.1	-86.5	-53.2	154.2	170.0	C2'-endo
C	-108.3	35.7	128.1	-158.2	-104.7	-48.7	176.3	142.3	C1'-exo
	-107.0	32.4	121.3	-159.8	-108.1	-53.1	178.5	131.5	C1'-exo
G	-85.3	45.6	146	-	-	-67.1	171.6	154.3	C2'-eno
	-82.6	43.4	146.2	-	-	-58.8	169.0	156.2	C2'-endo

[a] Parameters calculated using the 3DNA program [1]

Table S2. Local DNA Base-Pair Parameters[a] for the d(TCGCGAATTCGCG) Duplex in the Crystal Structures of the Wild-Type (Black) and A138T (Red) EcoRI Complexes

DNA Param. / Base-pair	Shear	Stretch	Stagger	Buckle	Propeller	Opening
$C_{-6}G_6$	0.30	-0.01	0.42	-24.96	0.55	-1.02
	0.15	0.01	0.38	-24.82	2.17	-1.39
$G_{-5}C_5$	-0.25	-0.16	-0.16	-4.08	-3.61	-4.20
	-0.17	-0.04	-0.15	-5.45	-3.76	0.62
$C_{-4}G_4$	0.10	0.02	-0.19	-1.60	-1.25	-4.44
	0.14	-0.11	-0.01	-0.37	-0.83	-4.42
$G_{-3}C_3$	-0.29	-0.10	-0.37	-10.90	0.88	-1.97
	-0.32	-0.08	-0.30	-13.55	-0.92	-1.09
$A_{-2}T_2$	0.13	0.01	-0.06	1.89	-0.80	-1.85
	0.13	-0.14	-0.10	-2.23	0.33	-3.30
$A_{-1}T_1$	-0.07	0.04	0.40	5.59	4.29	-0.28
	0.13	-0.02	0.58	4.58	5.62	0.44
T_1A_{-1}	0.07	0.04	0.40	-5.58	4.28	-0.29
	-0.12	-0.02	0.58	-4.58	5.61	0.43
T_2A_{-2}	-0.13	0.01	-0.06	-1.89	-0.80	-1.85
	-0.13	-0.14	-0.10	2.23	0.33	-3.31
C_3G_{-3}	0.29	-0.10	-0.37	10.90	0.88	-1.98
	0.32	-0.08	-0.30	13.55	-0.92	-1.10
G_4C_{-4}	-0.10	0.02	-0.19	1.60	-1.25	-4.44
	-0.15	-0.11	-0.01	0.37	-0.83	-4.40
C_5G_{-5}	0.25	-0.16	-0.16	4.08	-3.61	-4.18
	0.17	-0.04	-0.15	5.45	-3.76	0.61
G_6C_{-6}	-0.30	-0.01	0.42	24.95	0.55	-1.00
	-0.15	0.01	0.38	24.81	2.17	-1.36

[a] Parameters calculated using the 3DNA program [1]

Table S3. Local DNA Base Step Parameters[a] for the d(TCGCGAATTCGCG) Duplex in the Crystal Structures of the Wild-Type (Black) and A138T (Red) EcoRI Complexes

DNA Param. / Base Step	Shift	Tilt	Slide	Roll[b]	Rise	Twist
$C_{-6}G_{-5}$	-0.16	3.33	0.12	7.54	2.89	23.37
	0.16	2.65	0.40	6.45	2.91	22.96
$G_{-5}C_{-4}$	-0.43	-0.08	-0.35	1.24	3.40	35.58
	-0.94	-2.20	-0.25	0.10	3.24	35.81
$C_{-4}G_{-3}$	0.88	1.84	-0.26	0.37	3.74	36.59
	1.23	3.66	-0.48	1.34	3.65	37.36
$G_{-3}A_{-2}$	-0.92	-1.19	-0.16	-1.07	3.26	31.88
	-1.18	0.43	-0.04	0.21	3.25	32.20
$A_{-2}A_{-1}$	0.58	-4.55	0.40	30.82	3.92	20.52
	0.70	-7.17	0.39	27.97	3.69	21.24
$A_{-1}T_{1}$	0.00	-0.01	0.71	-53.84	4.96	44.78
	0.00	-0.01	0.72	-52.10	4.92	40.85
$T_{1}T_{2}$	-0.57	4.54	0.40	30.78	3.91	20.53
	-0.69	7.17	0.39	27.95	3.69	21.25
$T_{2}C_{3}$	0.92	1.19	-0.16	-1.07	3.26	31.88
	1.19	-0.43	-0.05	0.21	3.25	32.19
$C_{3}G_{4}$	-0.88	-1.84	-0.27	0.37	3.74	36.59
	-1.23	-3.67	-0.49	1.34	3.65	37.36
$G_{4}C_{5}$	0.43	0.08	-0.36	1.24	3.40	35.58
	0.94	2.20	-0.25	0.10	3.24	35.81
$C_{5}G_{6}$	0.15	-3.33	0.12	7.54	2.89	23.37
	-0.16	-2.65	0.39	6.45	2.91	22.97

[a] Parameters calculated using the 3DNA program [1]

[b] The hallmark of the EcoRI DNA kink [2], the large roll angles at the $A_{-2}A_{-1}$, $A_{-1}T_{1}$, and $T_{1}T_{2}$ base steps are identical in the nucleic acids from both structures.

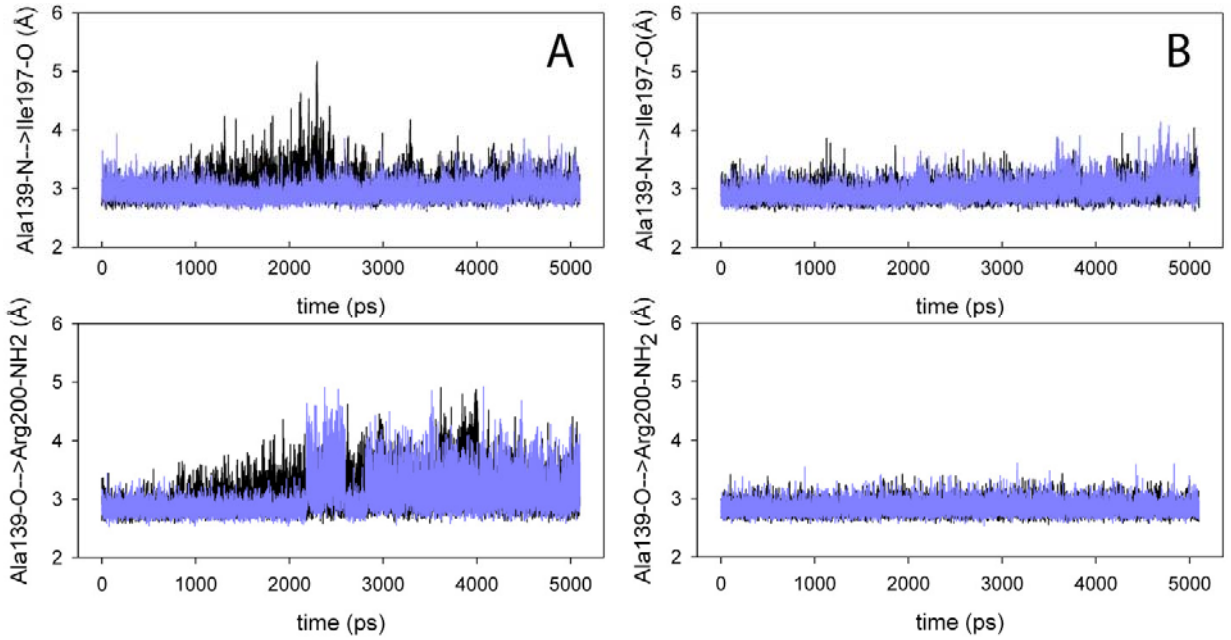

Figure S1. Molecular Dynamics Simulations Performed at 300K Reproduce Water41 Binding Site Protein-Protein Contacts Observed in the Wild-Type and A138T Crystal Structures

The two graphs in panel A refer to a 5 ns simulation of the wild type specific complex (starting from a refined version of crystal coordinates PDB accession code 1CKQ) and the graphs in panel B refer to a 5 ns simulation of the A138T complex (present work; PDB accession code 2OXV). Upper panels show distance (Å) from Ala139-N to Ile197-O. Lower panels show distances (Å) from Ala139-O to Arg200-guanidino. The black and blue traces refer to the distances in the two half-sites. In the case of the wild-type complex, these two protein-protein interactions stabilize the water41 binding site. Despite the absence of the analogous water molecule, we observe the same protein-protein contacts during the simulation of the A138T complex.

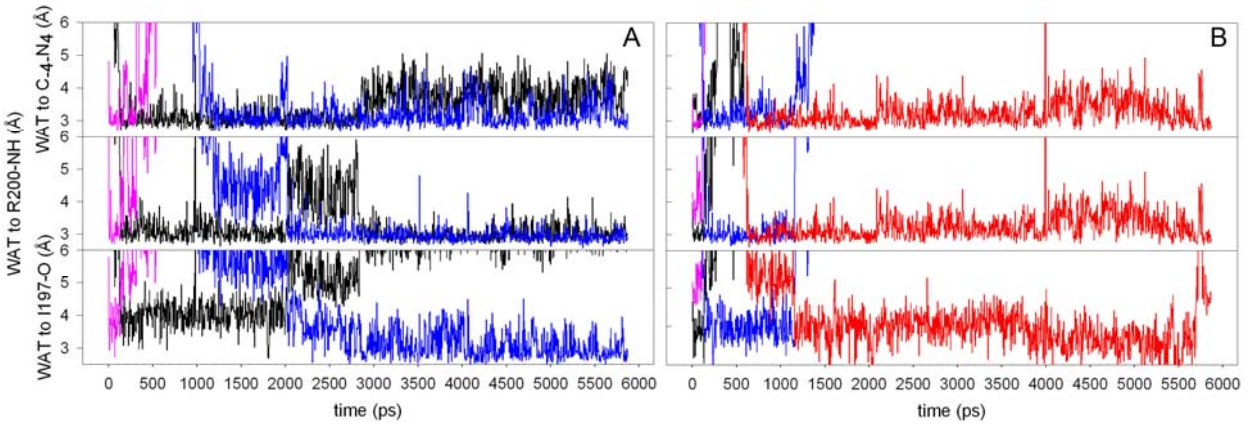

Figure S2. Water Molecules Are Free to Enter and Leave the Water41 Binding Site During Molecular Dynamics Simulations of the Wild-Type Complex

In this simulation, we stripped water41 from both half sites of the wild-type crystal structure (refined version of PDB accession code 1CKQ) and performed a 6 ns simulation of this complex in explicit solvent at 300K. Panels A and B describe the solvent dynamics within half-sites one and two, respectively. Three to four different solvent molecules (single water molecules are colored similarly in the three graphs within each panel) enter the water41 binding site from the bulk. These waters contact the same protein and DNA functional groups that water41 contacts in the crystal structure (see Figure 3A in the main text). After a brief (1 to 2 ns) equilibration period during which there is exchange between the binding site and bulk solvent, the binding sites (two subunits) are stably occupied by single water molecules. Note that the *protein-protein* contacts made by the residues that form the water41 binding site remain intact throughout the 6 ns simulation, 5 ns of which are shown in Figure S1.

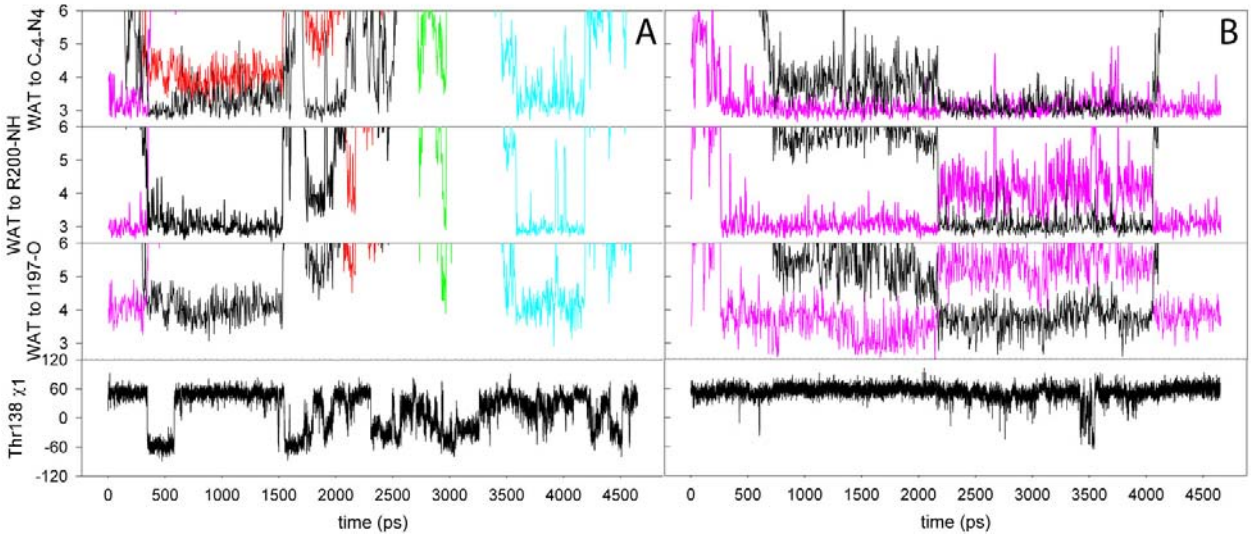

Figure S3. MD Simulation After In Silico Mutagenesis of Ala138 to Thr, Showing Dynamics of the Water41 Binding Site

For this simulation, we took the coordinates of the wild type specific complex (refined version of PDB accession code 1CKQ), changed Ala138 to Thr in both enzyme subunits, then performed molecular dynamics as described in the Experimental Procedures. Panels A and B plot the behavior of the first and second protein-DNA complex half-sites, respectively. For each panel, the first three graphs show the distances between water molecules and the three DNA/enzyme ligands that comprise the water41 binding site. The bottom graph shows the χ_1 side chain dihedral angle of Thr138. Within each half-site, we color waters similarly in the three graphs (i.e. In panel A, the cyan traces in the top three graphs refer to the same water molecule). In the first half-site (left), when Thr138 adopts the χ_1 value of ~-60° (the same rotamer that we observe in the X-ray crystal structure and during MD simulations (see Figure S5) of the A138T complex), water is ejected from the binding site. This is reminiscent of the crystal structure and MD simulations of the A138T complex, where the water41 binding site is not occupied (Figure 3, main text). In the second half-site, Thr138 samples the crystallographic rotamer for less than 50 ps and the water41 network remains intact, reminiscent of the wild type complex.

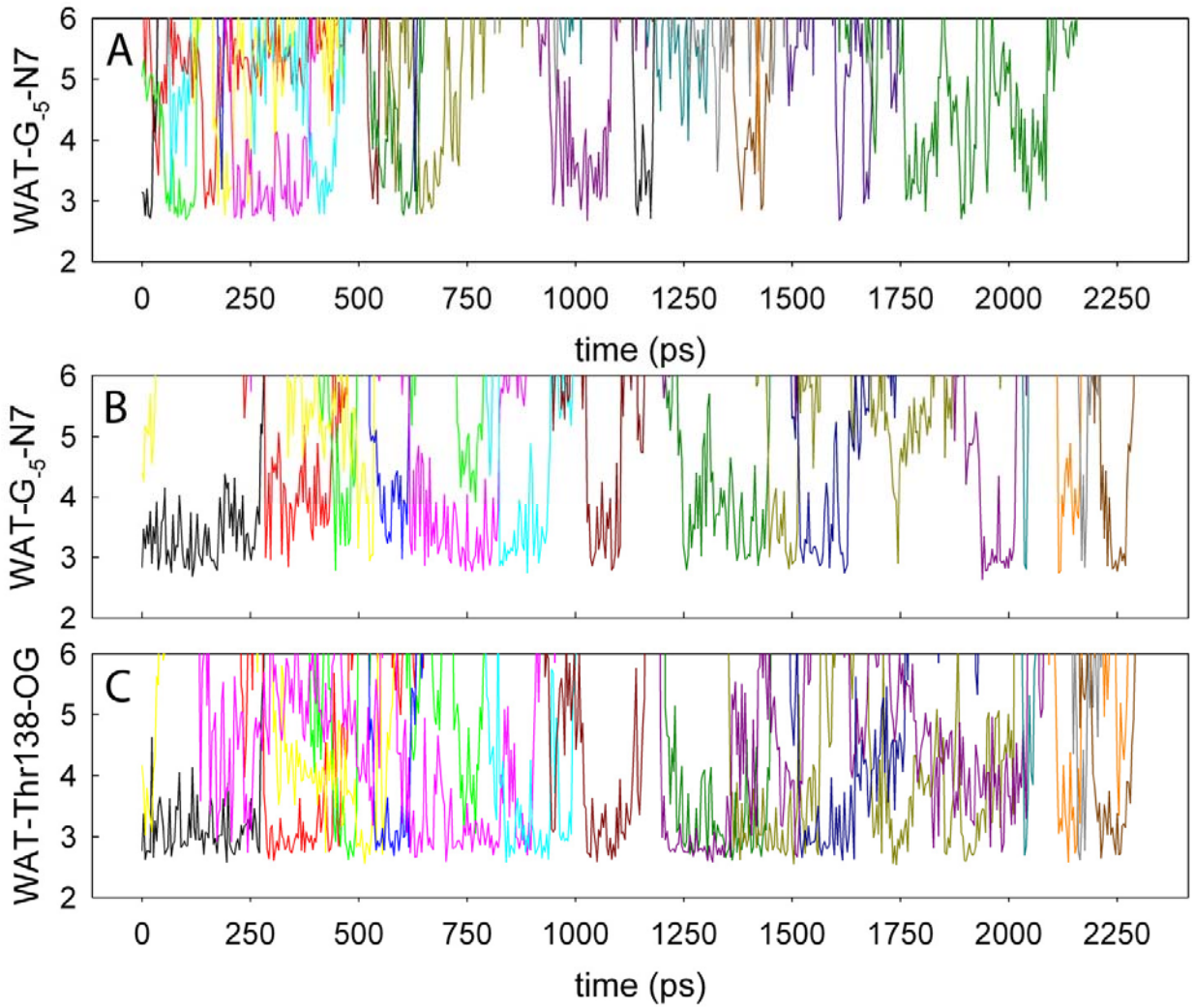

Figure S4. Water Residence Times at a G_{-5} Binding Site During MD Simulations of the Wild-Type and A138T Specific Complexes

In panel A, we use different colors to depict different waters that visit the G_{-5}-N7 binding site in the wild-type complex. Panels B and C describe the water mediated interaction between the Thr138 side chain hydroxyl group and G_{-5}-N7 (see Figure 3B main text for molecular rendering of the contact) during a MD simulation of the A138T complex. Waters are colored similarly in panels B and C (i.e. the black traces in B and C follow the same water molecule). Note that the presence of the bridging interaction in the A138T complex does not significantly increase the G_{-5}-N7 water residence times relative to the wild-type binding site.

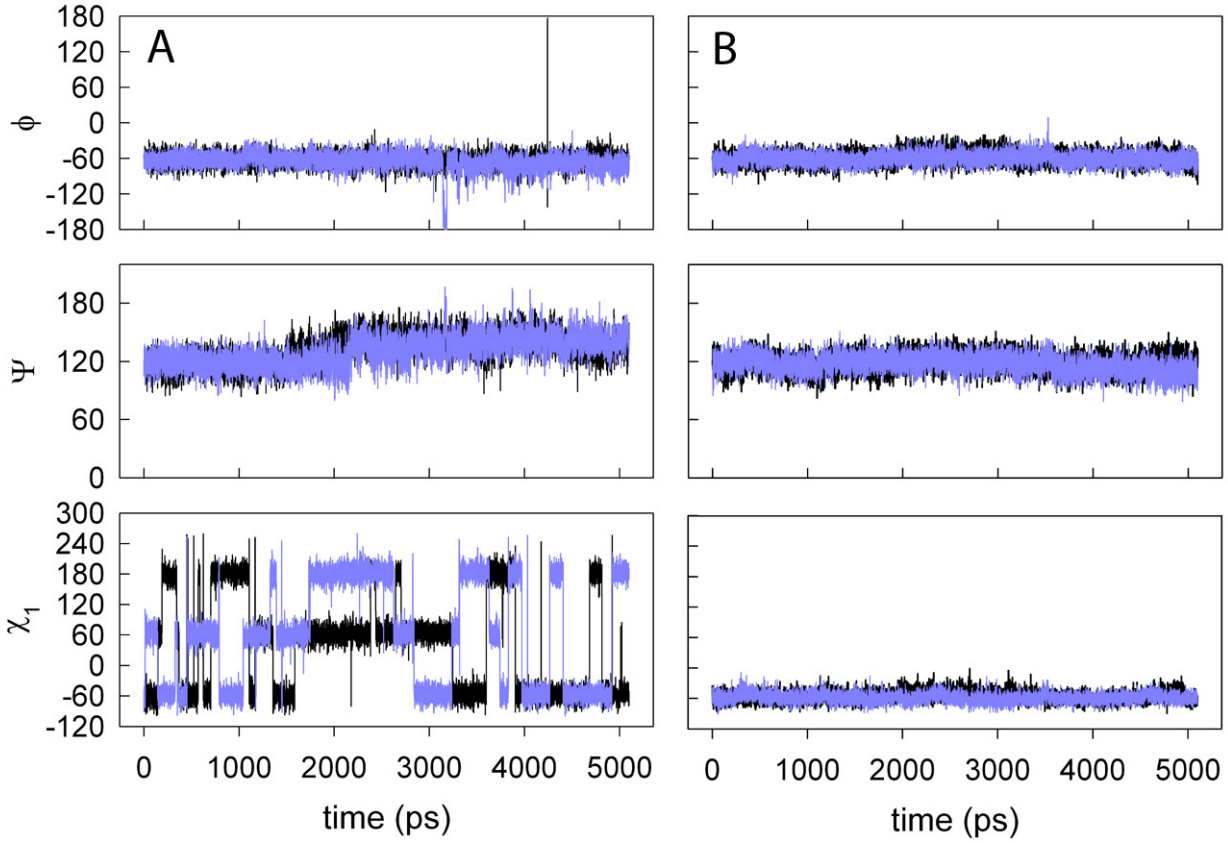

Figure S5. Comparison of Residue 138 Side-Chain Dynamics During Simulation of the Wild-Type (Left) and A138T Mutant (Right) Complexes

Panel A shows the ϕ, ψ, and χ_1 dihedral angles for Ala138 during a 5 ns molecular dynamics simulation of the wild type specific complex starting from a refined version of PDB accession code 1CKQ. Panel B shows the analogous dihedral angles for Thr138 during a simulation of the A138T complex (this work; PDB accession code 2OXV). Black and blue traces report on the behavior of the amino acids in the two subunits of each homodimer. Whereas the Ala138 side chain in the wild-type complex explores all three gauche configurations (bottom left panel), Thr138 is restricted to a single rotamer throughout the simulation (bottom right panel).

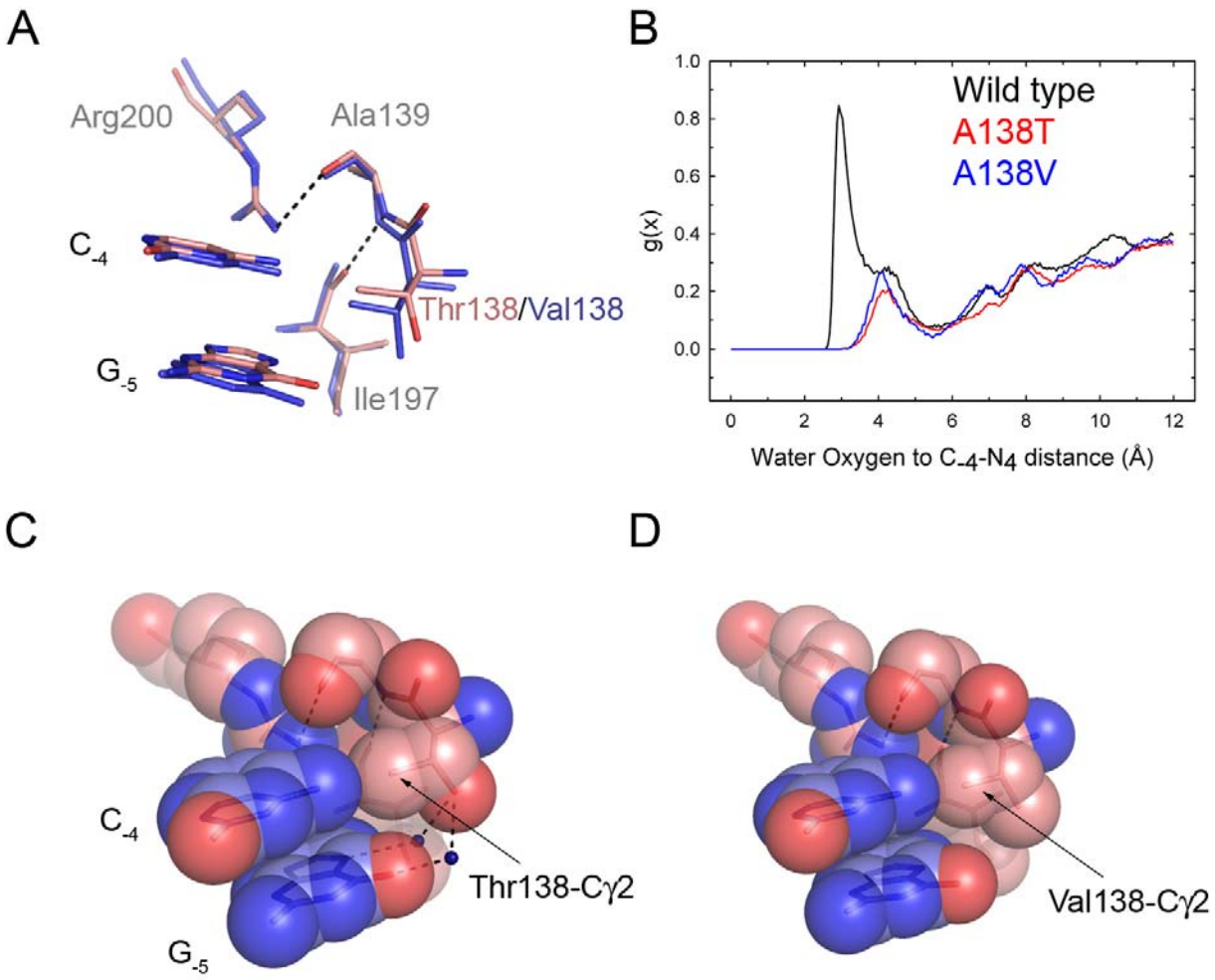

Figure S6. The A138V Mutation, Which Also Results in Relaxed Specificity [3], Has a Similar Effect on the Structure of the Specific Complex as the A138T Mutation

We changed Thr138 to valine in both subunits of the A138T crystal structure and performed a 2.75 ns molecular dynamics simulation on this specific complex. In panel A, we compare the A138T crystal structure with the structure of the A138V complex, calculated as an average over the course of the MD trajectory. The A138T complex is colored in CPK and the A138V complex is colored blue throughout. Note that the Thr138 and Val138 adopt similar conformations. In panel B, we plot the water oxygen to DNA functional group radial distribution function calculated over the course of wild-type, A138T, and A138V MD simulations. The lack of a water peak within hydrogen bonding distance of the DNA functional group in the A138V simulation shows that this substitution, like the A138T mutation, results in the loss of the water molecule bridging the protein to C_{-4}-N_4. van der Waals renderings shown for the A138T crystal structure (panel C) and the MD averaged A138V structure (panel D). Note that Thr138-Cγ2 and Val138-Cγ2 make analogous packing interactions with bases flanking the GAATTC recognition site.

Supplemental References

1. Lu, X. J. & Olson, W. K. (2003) 3DNA: a software package for the analysis, rebuilding and visualization of three-dimensional nucleic acid structures *Nucleic Acids Res* **31,** 5108-21.
2. Kim, Y. C., Grable, J. C., Love, R., Greene, P. J. & Rosenberg, J. M. (1990) Refinement of Eco RI endonuclease crystal structure: a revised protein chain tracing *Science* **249,** 1307-9.
3. Heitman, J. & Model, P. (1990) Mutants of the EcoRI endonuclease with promiscuous substrate specificity implicate residues involved in substrate recognition *Embo J* **9,** 3369-78.